IMECE2004-60334

MOLECULAR-DYNAMICS STUDY OF THERMAL BOUNDARY RESISTANCE: EVIDENCE OF STRONG INELASTIC SCATTERING TRANSPORT CHANNELS

Robert J. Stevens
Department of Mechanical and Aerospace Engineering
University of Virginia
Charlottesville, VA 22904
Rob_Stevens@virginia.edu

Pamela M. Norris
Department of Mechanical and Aerospace Engineering
University of Virginia
Charlottesville, VA 22904
Pamela@virginia.edu

Leonid V. Zhigilei
Department of Material Science and Engineering
University of Virginia
Charlottesville, VA 22904
lz2n@virginia.edu

ABSTRACT

With the ever-decreasing size of microelectronics, growing applications of superlattices, and development of nanotechnology, thermal resistances of interfaces are becoming increasingly central to thermal management. Although there has been much success in understanding thermal boundary resistance (TBR) at low temperature, the current models for room temperature TBR are not adequate. This work examines TBR using molecular dynamics (MD) simulations of a simple interface between two FCC solids. The simulations reveal a temperature dependence of TBR, which is an indication of inelastic scattering in the classical limit. Introduction of point defects and lattice-mismatch-induced disorder in the interface region is found to assist the energy transport across the interface. This is believed to be due to the added sites for inelastic scattering and optical phonon excitation. A simple MD experiment was conducted by directing a phonon wave packet towards the interface. Inelastic scattering, which increases transport across the interface, was directly observed. Another mechanism of energy transport through the interface involving localization of optical phonon modes at the interface was also revealed in the simulations.

Nomenclature

c = propagation speed of phonon, m/s
E = total kinetic energy of heating or cooling zone, eV
$g(\omega)$ = phonon density of states, s/m^3
$g'(\omega)$ = unscaled occupied phonon density of states, s/m^3
h_{BD} = thermal boundary conductance, W/m^{2}K
k_B = Boltzmann constant

L = number of atoms in an atomic plane
m = mass of individual atoms, m/s
$n(\omega,T)$ = phonon occupation distribution function
N/V = atom number density, 1/m^3
$\dot{q}$ = heat flux across interface, W/m^2
Q = energy to be added each time step, eV
r = length, m
R_{ij} = distance between atoms i and j, m
T = temperature, K
u_{total} = energy per unit volume of subsystem, J/m^3
U = total potential energy of atomic system, eV
U_{LJ} = LJ pair interaction function, eV
v = velocity of individual atoms, m/s
α = phonon transmission coefficient
ε = LJ energy parameter, eV
ϕ = phonon incidence angle
$\hbar$ = Planck's constant, Js
σ = LJ lattice parameter, m
ω = angular frequency, 1/s

Subscripts

$1,2$ = side one or two of an interface
A,B = side A or B
ij = atom pair index
j = phonon mode
l = longitudinal phonon mode
new = value for next time step
old = value of previous time step
t = transverse phonon mode

Introduction

Thermal management has played a critical role in the development of micro and optoelectronic devices over the past several decades. Much of the theory used in thermal management design has relied on macroscopic principles, where feature sizes and times are much larger than the mean free path and scattering time of the energy carriers. Only recently, with the advent of smaller devices and structures, have we had to develop models and theories based on microscopic principles. This is particularly the case with the growing interest in nanoscale and superlattice devices, where TBR can have a major impact on the overall thermal characteristics and performance of the devices. The TBR can vary widely depending on the fabrication technique and types of materials utilized. Precise knowledge of the TBR is required in order to understand fully the thermal characteristics of nanodevices and minimize the uncertainties in their design and performance.

Thermal boundary resistance creates a temperature drop, ΔT, across an interface between two different materials when a heat flux is applied. This was first observed by Kapitza for a solid and liquid helium interface in 1941 [1]. The inverse of TBR is often referred to as Kapitza conductance, h_{BD}, or thermal boundary conductance, TBC. The heat flux, $\dot{q}$, across an interface can be expressed by the following equation:

$$\dot{q} = h_{BD}\Delta T \qquad (1)$$

At low temperatures, the thermal diffusivity of dielectric materials is often relatively high because of the increasing scattering times and mean free paths of the thermal energy carriers (acoustic phonons). At these low temperatures, TBR can start restricting heat transport and must be considered in designing thermal management strategies.

Unlike at low temperature, at room temperature the energy carriers' mean free paths are quite small ($\sim$10-100 nm) and the TBR is typically neglected because it is insignificant as compared to the thermal resistance of the bulk material. It is only recently, with the advent of nanoscale devices, the TBR started to be considered as a significant source of thermal resistance at room temperature. This is especially the case for devices with multiple interfaces such as superlattices [2] and very large scale integrated (VLSI) circuits. Specific applications where TBR is currently being considered are thermoelectrics [3, 4], thin-film high temperature superconductors [5, 6], vertical cavity surface emitting lasers [7], and optical data storage media [8]. More applications are sure to follow.

Although the first measurement of thermal boundary resistance was reported in 1941 by Kapitza for He-solid interfaces [1], it was not until 1952, when the first theoretical description of the phenomenon was suggested by Khalatnikov [9]. The description, currently known as the acoustic mismatch model (AMM), predicts poor phonon transport across interfaces when there are large differences in the density and sound velocity for the two interface materials, as is the case for the interface between liquid helium and most solids. Although the model does predict significant temperature differences in the range of 1 K, the AMM tends to overpredict thermal boundary resistances for He-solid interfaces by as much as two orders of magnitude. It is not until around 100 mK, when the AMM becomes more inline with experiments but still off by a factor of three [10, 11]. Much of the deviation between theory and experiment has been attributed to surface contamination and defects that may increase phonon coupling between the He-solid. In fact, when extreme care was taken to create an ideal interface, experiments tended to measure phonon transmissions closer to those predicted by AMM. For a summary of such experiments see Swartz and Pohl [10].

The AMM was extended to solid-solid interfaces by Little in 1959 [12]. Early work done in the 1960's and 1970's on sapphire and indium interfaces at low temperatures ($\sim$1 K) showed that the measured resistances were greater than the AMM prediction [10]. More recently, in 1987, Swartz measured TBR for several metal film and dielectric interfaces up to a temperature of 200 K [13]. Swartz found that below $\sim$40 K there was good agreement between the model and experiment, but above 40 K the model tended to underpredict the measured TBR.

The AMM theory is based on the assumption that each solid can be treated as a continuum with a perfect interface. The incident phonons are treated as plane waves, for which transmission and reflection probabilities are calculated, and there is no scattering at the interface. The AMM assumptions are generally reasonable at low temperatures ($<$10 K) and for perfect interfaces. However, at higher temperatures and for non-perfect interfaces, where higher frequency phonons dominate the heat transport, scattering is highly probable. In 1986, Eisenmenger experimentally determined that there was strong scattering at interfaces for phonons with frequencies above a few hundred GHz for liquid He and Si interfaces [14]. In order to account for the phonon scattering at interfaces, the diffuse mismatch model (DMM) was suggested in 1987 by Swartz and Pohl [13]. The model assumes that all phonons incident on the interface from both sides are elastically scattered and then are emitted to either side of the interface. The probability for a phonon to be emitted to a particular side is proportional to the phonon density of states (DOS) of the two materials. Inherent to the DMM is that the transport is independent of the interface structure itself and is only dependent on the properties of the two materials. DMM also assumes only elastic scattering takes place at the interface; that is, for each phonon incident on the interface a single phonon with the same frequency will scatter from the interface. The elastic scattering assumption, as opposed to inelastic scattering, does not allow phonons to scatter into multiple lower frequency phonons or multiple phonons to scatter into higher frequency phonons. In the case of low temperature liquid He to solid interfaces the DMM predicts TBR two orders of magnitude lower than the one predicted by the AMM, while for solid-solid interfaces the differences are small [10].

Both mismatch theories can be expressed mathematically as [10]

$$h_{BD,1} = \frac{1}{2}\sum_j \frac{\partial}{\partial T} \int_0^{\pi/2} \int_0^{\varpi_{max}} g_{1,j}(\omega) n(\omega,T)\hbar\omega c_{1,j} \qquad (2)$$
$$\times \alpha_{1,j}(\phi,j,\omega)\cos(\phi)\sin(\phi)d\omega d\phi$$

where $h_{BD,1}$ is the thermal boundary conductance from side 1 to side 2, $g_{1,j}(\omega)$ is the phonon DOS per unit volume of mode j on side 1, $n(\omega,T)$ is the occupancy distribution function, $\hbar$ is Planck's constant, ω is angular frequency, ω_{max} is the maximum phonon frequency on side 1, $c_{1,j}$ is the phonon propagation velocity in side 1 for phonons of mode j, $\alpha_{1,j}$ is the transmission coefficient incident on the interface from side 1 of mode j, and ϕ is the phonon incidence angle. The occupancy distribution function for phonons is the Bose-Einstein distribution function

$$n(\omega,T) = \frac{1}{\exp\left(\hbar\omega/k_B T\right) - 1} \tag{3}$$

where k_B is the Boltzmann constant.

The summation in Eq. (2) is taken over all phonon modes, which is normally restricted to the acoustic branches. The difference in the AMM and DMM is how the transmission coefficient is calculated. This can be quite involved for the AMM where the transmission coefficient is dependent on θ. For the DMM case, where complete diffuse scattering is assumed, the transmission coefficient is independent of θ and can be expressed as [10]

$$\alpha_{1,j}(\omega) = \frac{c_{2,j} g_{2,j}(\omega)}{c_{2,j} g_{2,j}(\omega) + c_{1,j} g_{1,j}(\omega)} \tag{4}$$

A few recent theoretical efforts for high temperature TBR modeling have been undertaken to modify the AMM and DMM theories [5, 15, 16]. Although there has been some success with the DMM and its derivatives, an important inherent limitation of DMM is that only elastic phonon scattering at the interface is considered. Recent experimental data indicate that the DMM is not sufficient to describe the true nature of room temperature processes at interfaces [17, 18]. Alternative models have been developed to describe other scattering mechanisms, including electron-phonon inelastic scattering at the interface [19-21] and electron-phonon scattering in the bulk [22]. To date there has been limited experimental data to validate the proposed models. This is primarily due to the extreme difficulty in making accurate and reproducible measurements, limited ability to change systematically one variable at a time, and complications in fully characterizing the interface. In this situation, computational investigation of TBR under well-controlled conditions provides an attractive complementary approach that may help in interpretation of experimental data and design of predictive theoretical models.

Early computational works used lattice-dynamical calculations to determine the transmission coefficients for the DMM [23-26] under assumptions of harmonic oscillations and elastic scattering. Molecular dynamic simulations began to be used in the late 1990's as a means of understanding thermal boundary conductance in more realistic anharmonic crystal models. One of the earliest MD simulations by Pickett *et al.* [27] was aimed at the investigation of the high thermal conductance in chemically vapor deposited diamond films. In 1997, Maiti *et al.* performed MD simulations to gain insight into the TBR across Si grain boundaries [28]. Daly *et al.* used MD to examine thermal conductivity of a superlattice, where TBR can be significant [29]. They found that interfacial roughness of a few monolayers resulted in a significant increase in the TBR of the interfaces. Schelling *et al.* utilized MD to determine phonon transmission coefficients as a function of phonon frequency using the Stillinger-Weber potential [30]. They demonstrated a good agreement between their model and AMM for low frequency phonons, but found large deviations for the high-energy phonons that dominate the heat transport at room temperature. Twu and Ho have done some preliminary work on the impact of interface disorder on TBR [31]. Although MD studies of TBR have been limited so far to a few simple interfaces, there is tremendous potential to conduct systematic simulation experiments to understand better the general physics of transport across ideal interfaces as well as the role of interface disorder and defects in TBR.

MD simulations are well suited for studying TBR at temperatures well above the Debye temperatures of interface materials. In real materials at temperatures above the Debye temperature, θ_D, the population of the phonon states increases linearly with temperature ($dn(\omega,T)/dT \sim 1$ for $T > \theta_D$). This is the case for MD simulations, where the assumption is that the particles behave classically so that the phonon modes too are populated linearly with temperature.

In this work, we perform MD simulations of the energy transport across an interface between two crystals with a pair-wise Lennard-Jones potential used to describe interatomic interaction. Atomic masses, strength of interatomic interaction, and the lattice parameter are methodically altered to investigate the effect of the phonon spectra and acoustic mismatch at the interface on TBR. Investigation of the energy transfer through a perfect interface is followed by examining the effect of various defects in the interface region on thermal transport.

Molecular Dynamics Simulations

The basic MD approach for determining the thermal boundary conductance of an interface is to create an interface of two crystal types (type A and type B) and to generate a temperature gradient across the interface sample. This leads to a temperature drop at the interface, which can then be used to calculate the thermal boundary conductance for a given interface using Eq. (1).

In this work, an interface was created between two FCC crystals as shown in Fig. 1. The interface was oriented on the (001) crystallographic plane. The pair-wise Lennard-Jones (LJ) potential was used to describe interatomic interaction in both parts of the system. The total potential energy of a system of N atoms is defined as

$$U = \sum_{i=1}^{N} \sum_{j>i}^{N} U_{LJ}\left(R_{ij}\right) = \sum_{i=1}^{N} \sum_{j>i}^{N} 4\varepsilon\left[\left(\frac{\sigma}{R_{ij}}\right)^{12} - \left(\frac{\sigma}{R_{ij}}\right)^{6}\right] \tag{5}$$

where U_{LJ} is the LJ pair interaction function, R_{ij} is distance between atoms i and j, and ε and σ are parameters defining the energy and length-scales of the potential function. Parameters for the interaction between atoms of different types were defined using the Lorentz-Berthelot rules, $\varepsilon_{AB} = \sqrt{\varepsilon_{AA}\varepsilon_{BB}}$ and

$\sigma_{AB} = (\sigma_{AA} + \sigma_{BB})/2$. Although LJ potential provides a realistic description of only a limited number of real systems (inert gases, van der Waals interaction in molecular systems), it is often used to model general effects rather than properties of a specific material. In this work, we use LJ potential with different sets of parameters to perform a systematic investigation of the basic physical processes responsible for TBR.
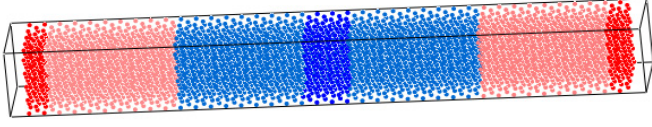

Fig. 1 Computational cell used to simulate thermal boundary resistance. Atoms of type A are shown in red and atoms of type B are shown in blue. The dark red and dark blue atoms belong to the heating and cooling zones, respectively.

Most of the data presented in this paper is in reduced units in reference to the LJ potential parameters for atoms of type A (left side of the interface). The length, energy, temperature, time, frequency, and thermal boundary conductance are defined in reduced units as:

$$r^* = r/\sigma, \qquad E^* = E/\varepsilon, \qquad T^* = k_B T/\varepsilon,$$
$$t^* = t \times \sqrt{\varepsilon/(m\sigma^2)}, \qquad \omega^* = \omega \times \sqrt{(m\sigma^2)/\varepsilon},$$
$$h_{BD}^* = h_{BD}\frac{m^{1/2}\sigma^3}{\varepsilon^{1/2}k_B} \qquad (6)$$

where m, σ, and ε are mass and LJ parameters of atom A. The "*" is not used in the remaining text and reduced units are implied unless specified otherwise.

Each side of the interface was made of 5x5x20 unit cells for a total of 2000 atoms and 40 atomic planes of each atom type. Simulations were run on larger structures, but no noticeable differences were observed, while simulations for smaller structures gave differing results. Periodic boundary conditions were used in all directions. Periodic conditions used in the z-direction (normal to the interface), simulate an infinite array of parallel interfaces with heating and cooling zones located in the middle of crystallites A and B respectively. This approach allows for an easier control over the total pressure in the system as compared to an alternative approach used by Twu and Ho, where the system was constrained within two rigid walls [31].

The equations of motion for all atoms in the system were integrated using the Nordsieck fifth-order predictor-corrector algorithm. In general, simulations consisted of equilibration of the initial structure at some specified temperature, followed by introduction of a constant heat flux through the system. The later was achieved by adding equal amounts of thermal energy per unit time in the heating zone and removing it from the cooling zone. The heating zone consisted of six atomic planes

in the middle of the type A crystal, while the cooling zone consisted of six atomic planes in the middle of the type B crystal. Larger heating and cooling zones were simulated, but no noticeable difference was observed with the six atomic plane simulations. Heat was added and subtracted from the heating and cooling zones respectively by adjusting the velocities of the atoms in each zone as follows:

$$v_{new} = v_{old}\left(1 \pm \frac{Q}{E}\right)^{1/2} \qquad (7)$$

where Q is amount of energy added (+) or removed (-) during each time step and E is the total kinetic energy of the zone being heated or cooled. Note that Eq. (7) does allow for some net change in momentum during a single time step, but the net momentum change vanishes because of averaging over several time steps.

After the initiation of heating and cooling, the system was allowed to reach steady state conditions. For most simulations, this took approximately 300,000 time steps or less. The simulations were continued for another 200,000 time steps for averaging purposes. The time steps were approximately 4×10^{-3} in reduced units. The overall system pressure was held constant throughout the simulations using the Berendsen barostate scheme [32]. The energy error over the entire simulation period did not exceed 0.1% once the system reached steady state, and was significantly less in most cases.

The temperatures for the 80 atomic planes were determined by

$$T = \frac{1}{3k_B N}\sum_{i=1}^{L} m_i v_i^2 \qquad (8)$$

where k_B is Boltzmann constant, L is the number of atoms in the atomic plane of interest, and m_i and v_i are the mass and velocity of atom i. A typical temperature distribution observed in the steady state regime is shown in Fig. 2. There is a dramatic temperature drop at the interface as is expected.

The thermal boundary resistance was calculated by first performing a linear curve fit to the temperature distribution for both parts of the system and then looking at the difference between these curve fits at the interface. The two atomic planes on either side of the interface and heating/cooling regions were not included in the linear curve fitting. This strategy, similar to the one used by Twu and Ho [31], is depicted in Fig. 2. The data points in the immediate vicinity of the interface and the heating/cooling zones were excluded when doing the linear fits to eliminate the effect of the heating/cooling method on the simulation results.

Results

Three series of interfaces were investigated. The first series was performed for an interface separating two materials with identical LJ parameters but different atomic masses. The second series examines TBR of lattice mismatched non-epitaxial interfaces, while the third series explores the impact of alloying at the interfaces.
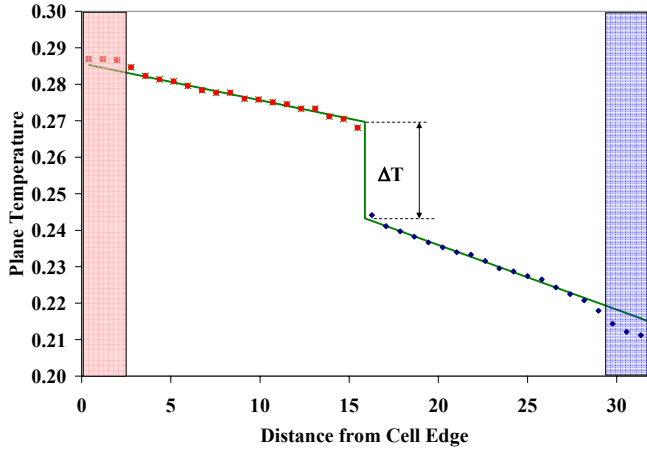
Fig. 2 Typical temperature profile observed in a MD simulation of thermal boundary resistance. Red dots are for atoms of type A and blue dots are for atoms of type B. Area in the shaded red and blue are the atomic planes that are heated and cooled respectively. The figure shows how ΔT is defined for h_{BD} calculations.
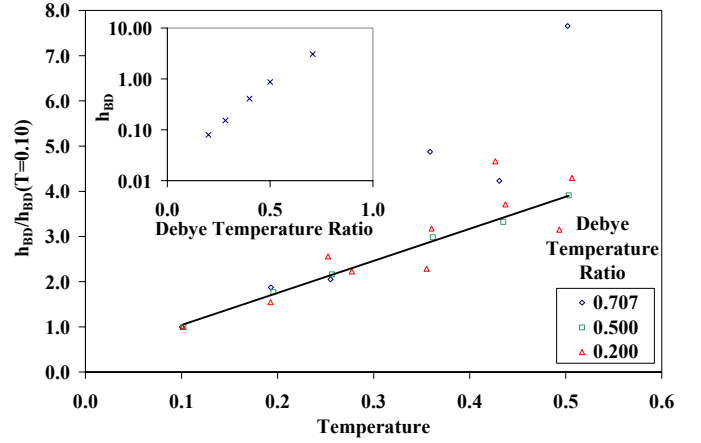

Fig. 3 Thermal boundary conductance as a function of temperature for three different interfaces with Debye temperature ratios of 0.2, 0.5, and 0.707. Temperature and h_{BD} are expressed in reduced units. The line is simply a guide for the eye to show approximate linear relationship. The thermal boundary conductances are normalized to the conductance value at T=0.1. The figure inset shows the thermal boundary conductance as a function of the ratio of Debye temperatures of the two materials forming the interface.

Mass mismatch series

In this series of simulations, the effect of mass mismatch between atoms of type A and B on h_{BD} is determined. Changing the mass of atoms directly affects the vibrational (phonon) spectrum of the crystal, which makes this series ideal for the investigation of the effect of phonon frequency mismatch on h_{BD}. Frequencies of atomic vibrations are inversely proportional to $m^{1/2}$, so that the ratio of Debye temperatures for any two simulated atom types is equal to $(m_A/m_B)^{1/2}$. The ratio of Debye temperatures is a qualitative indicator of how well the phonon spectra of the two sides overlap. Figure 3 shows the results of a series of simulations for Debye temperature ratios of 0.2, 0.5, and 0.707 versus temperature. The h_{BD} values are normalized to the h_{BD} at T=0.1 in order to see the trends for all three interfaces on a single plot. The values of h_{BD} at T=0.1 for the Debye temperature ratios of 0.2, 0.5, and 0.707 are 0.031, 0.403, and 1.49 respectively. Of immediate interest is that h_{BD} is not constant and appears to increase linearly with temperature in the cases where the Debye temperature ratio is 0.2 and 0.5. An increase of h_{BD} with temperature has also been reported by Twu and Ho [31]. These results differ from the mismatch models that predict temperature-independent TBR above the Debye temperature.

The inset of Fig. 3 shows h_{BD} versus Debye temperature ratio at T= 0.26, the temperature of the interface. There is more than one order of magnitude difference between h_{BD} for the samples simulated. This result is consistent with the DMM, but has not been observed experimentally at high temperatures yet.

To compare the results of MD simulations with DMM, the phonon DOS and phonon propagation speeds must be obtained. The phonon DOS was determined by Fourier-transforming the velocity-velocity autocorrelation function. The spectra was scaled under the harmonic approximation by noting that the energy per unit volume of a subsystem can be expressed as

$$u_{total} = \int_0^{\omega_{max}} g(\omega)n(\varpi,T)\hbar\omega d\omega \qquad (9)$$

$$= \int_0^{\omega_{max}} Cg'(\omega)T\hbar\omega d\omega = \frac{3Nk_BT}{V}$$

where $g(\omega)n(\omega,T)$ can be expressed as $Cg'(\omega)T$ in the MD case and where C is the scaling factor, $g'(\omega)$ is the unscaled spectrum, and N/V is the atom number density. Phonon DOS were calculated at several different temperatures to see that $g'(\omega)$ was in fact not a function of temperature. This was the case except for very low temperatures. This technique does not separate the phonon spectra into individual modes. The phonon propagation velocity is determined by generating phonon wave packets as described by Schelling *et al.* [30] and adjusting the initial velocity in order to obtain a coherent propagating wave packet.

Figure 4 shows the dependence of the DMM transmission coefficient on ω calculated using Eq. (4) and the phonon spectra and propagation speeds for an interface with a mass ratio of 1:4 (Debye temperature ratio of 0.5). Since the phonon spectra were not broken into individual modes, the effective phonon propagation velocity was assumed to be

$$c_{eff} = \frac{c_l + 2c_t}{3} \qquad (10)$$

where the subscript l and t are for the longitudinal and transverse modes. The velocity was assumed to be wavelength independent.
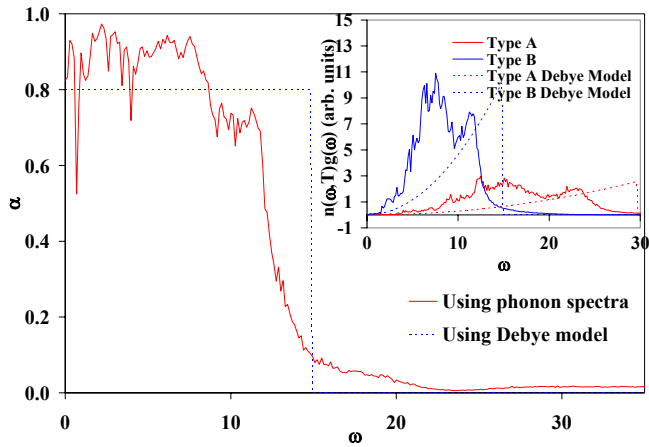
Fig. 4 Phonon transmission coefficient calculated for DMM, Eq. (4), using phonon DOS and speeds calculated from MD simulations for an interface with a mass ratio of 0.25. DOS's were obtained by performing a Fourier transform on the velocity-velocity autocorrelation function at T≈0.26. The inset shows the phonon DOS for both atom types. Also shown is the Debye model DOS where the cutoff frequencies were determined using the calculated phonon propagation speeds.

Fig. 5 Ratio of MD h_{BD} to DMM h_{BD} as a function of temperature for three different interfaces. The inset shows the ratio MD h_{BD} to DMM h_{BD} as a function of the ratio of the Debye temperatures for the two materials at T≈0.26. The data for the inset is for mass and energy series.

The dashed line indicates the Debye model transmission coefficient for the interface. The inset in Fig. 4 shows the phonon DOS for both simulated FCC structures along with the Debye model DOS where the cutoff frequencies were determined using the calculated phonon propagation speeds.

The calculated transmission coefficient and phonon DOS are used in Eq. (2) to calculate the DMM h_{BD} for the interfaces simulated. As noted earlier, the DMM h_{BD} is independent of temperature. Figure 5 shows the ratio of the simulated h_{BD} to the DMM h_{BD}. The DMM does not completely capture transport across an ideal interface. The discrepancy between the simulated and theoretical values approaches a factor of two or more at higher temperatures. The most likely explanation for this discrepancy is that the DMM accounts only for elastic scattering, while MD accounts for both elastic and inelastic scattering at the interface. The linear temperature dependence indicates a scattering process that is proportional to phonon population, since the phonon population increases linearly with temperature at high temperatures. In the classical limit, at temperatures above the Debye temperature, it appears that inelastic scattering provides the major contribution to the energy transport across the interface, surpassing the contribution of the elastic scattering. This conclusion is further supported and discussed in more detail in the last section.

The inset in Fig. 5 shows the ratio of the MD h_{BD} to the DMM h_{BD} versus Debye temperature ratio at T≈0.26. It is apparent that for ideal interfaces the DMM tends to underpredict h_{BD}, especially at high temperatures. These results are different then observed experimentally on real interfaces by Stevens *et al.* [18] and Stoner and Maris [17]. These results also counter the arguments made by Stoner and Maris in attempts to explain discrepancies between the measured h_{BD} and the ones predicted by DMM for Pd-diamond interfaces [17]. They attributed larger than expected values of h_{BD} measured for Pd-diamond interfaces to a strong coupling
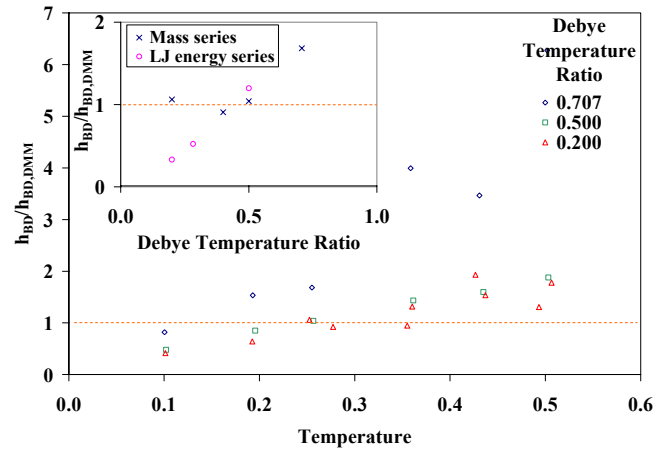
between atoms of different type at the interface. By varying the LJ energy parameter ε and setting all other parameters equal in both parts of the system, results similar to the mass mismatch are obtained as shown by circles in the inset in Fig. 5.

Lattice mismatch series

To better understand the impact of defects on h_{BD}, an interface was created with a lattice mismatch ratio of $\sigma_A/\sigma_B = 0.8$. Part A of the system had 5×5×20 unit cells and part B had 4×4×20 unit cells. Relaxation of the interface at T=0.42 for a time of 65 followed by quenching for a time of 45 resulted in a formation of a thin disordered layer at the interface, Fig.6. Simulations were conducted in a similar fashion as those for the mass mismatch series discussed above. Figure 7 illustrates the temperature dependence of h_{BD} for the lattice mismatch interface for which the atomic mass and the energy parameter ε are identical for both types of atoms. Similarl to the results discussed above, one can see the increase in h_{BD} with temperature. The h_{BD} values in Fig. 7 are divided by the DMM h_{BD} calculated from the simulated phonon DOSs and speeds. The DMM appears to overpredict the values of h_{BD} for the
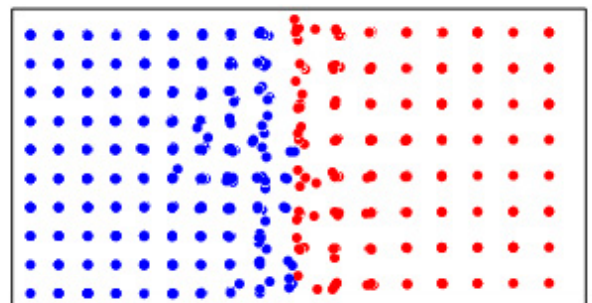

Fig. 6 A section of a relaxed atomic structure of an interface created by combining two crystals with a lattice mismatch of $\sigma_A/\sigma_B = 0.8$.
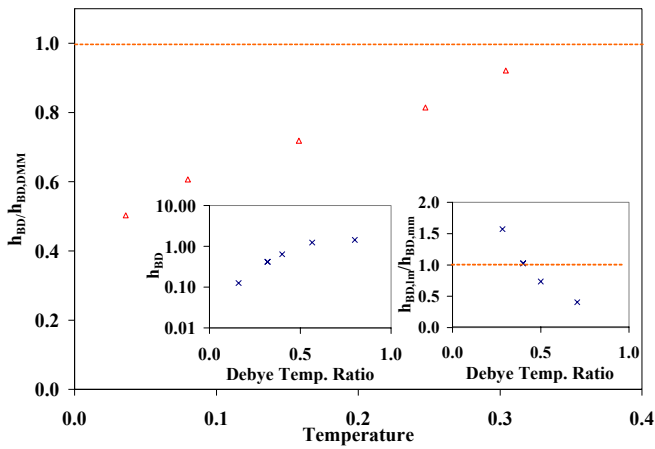
Fig. 7 Ratio of MD h_{BD} to DMM h_{BD} as a function of temperature for an interface with a lattice mismatch of $\sigma_A/\sigma_B = 0.8$. The first inset shows h_{BD} versus Debye temperature ratio for the lattice mismatch MD simulation with $\sigma_A/\sigma_B = 0.8$ and T≈0.26. The Debye temperature ratio is controlled by changing the mass ratio of atoms of type A and B. The second inset shows the h_{BD} for the series illustrated in the first inset divided by the h_{BD} calculated for the same Debye temperature ratios but without lattice mismatch ($\sigma_A/\sigma_B = 1$).

temperature range simulated in this particular series. This observation is somewhat expected since the phonon speeds and the DOSs are nearly identical for the two parts of the system in this lattice mismatch series.

Simulations were also performed for a series where the mass mismatch was combined with the lattice mismatch. The first inset of Fig. 7 shows h_{BD} as a function of Debye temperature ratio. The observed dependence is similar to the mass mismatch series, except for the case of large Debye temperature ratio interface, where h_{BD} plateaus for the lattice mismatch series. This indicates that scattering at the interface for similar materials dominates the transport resistance, while for dissimilar materials an additional interface scattering appears to assist the energy transport. These results differ from those reported by Petterson and Mahan for lattice-dynamics simulations that were restricted to elastic scattering and very ordered interfaces [24]. Petterson and Mahan modeled interfaces that had perfect crystal structures on both sides of the interface.

To illustrate the impact of the disordered layer caused by lattice mismatch on the boundary conductance, the results obtained for systems with both lattice and mass mismatch are divided by the values of h_{BD}'s calculated for the same Debye temperature ratios but without the lattice mismatch. The results are shown in the second inset of Fig. 7. It appears that the disordered layer at the interfaces assist in thermal transport for interfaces with small Debye temperature ratios, while hindering transport for large Debye temperature ratios.

Interface alloying series

Another type of interface structure considered was generated by randomly mixing atoms in the two atomic layers

adjacent to the interface, Fig. 8. Figure 9 shows the results of the simulations performed on such "alloyed" interface at T≈0.26. The results are divided by the predictions of DMM and the results from the mass mismatch series and plotted versus Debye temperature ratio. In all cases, the alloying resulted in a relatively small improvement of the energy transport across the interface. This result is different than that obtained by Twu and Ho [31]. Twu and Ho used the Morse potential on one side of the interface and ran the simulations at T=0.3.

The impact of individual point defects was also considered by removing one atom from the type A side of an ideal interface. There were no noticeable changes in the h_{BD} over the range of mass mismatches tested in the first series. This indicates that individual point defects that might be found in epitaxially grown films might contribute little to the overall thermal boundary resistance.
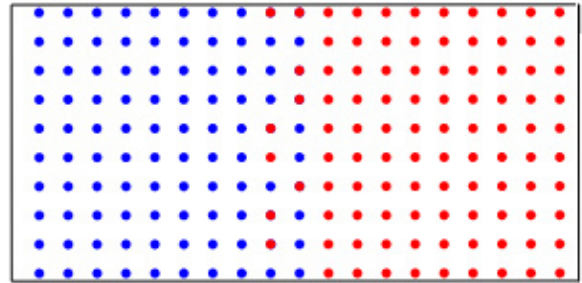

Fig. 8 A section of the alloyed interface produced by mixing atoms in the two atomic layers adjacent to the interface.
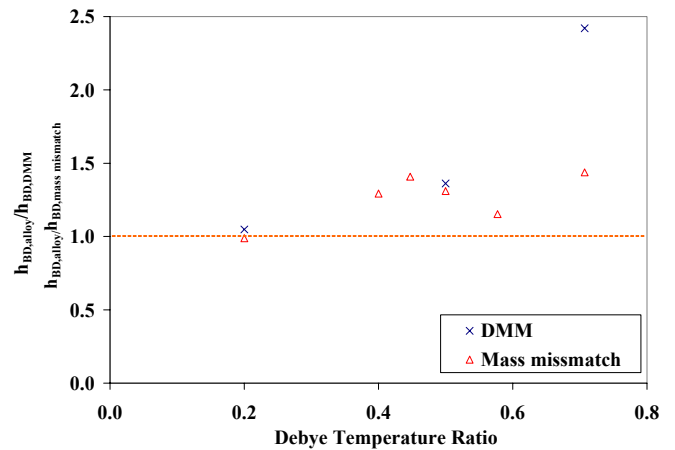

Fig. 9 Thermal boundary conductance as a function of the ratio of Debye temperatures for the "alloyed interface" series. The results are divided by the values predicted by the DMM and the results obtained for an ideal interface in the mass mismatch series.

Evidence of inelastic scattering

The temperature dependences of the thermal boundary conductance observed in the above series suggest that inelastic scattering is likely the dominant mechanism of energy transport

7

across interfaces. In order to provide a direct verification of this hypothesis, we performed a number of MD computer experiments aimed at direct observation of the inelastic phonon scatting. In these simulations, performed at the initial zero temperature and mass ratio between the atoms of type A and B of 0.2, a longitudinal phonon wave packet was introduced into one side of the interface in the fashion described by Schelling *et al.* [33]. The frequency of the phonon was set to ω=13.6. The DMM predicts a transmission coefficient of 0.2% at this frequency. The wave packet was initially centered at atomic plane 65 and directed towards the interface, which was located between atomic planes 119 and 120.

Figure 10(a) shows the displacement of the atomic planes 90, 119, 120, and 122. The phonon wave packet can be seen passing through the atomic planes in route to the interface between time 0.0 and 0.4. At about t=0.3 the phonon wave packet starts to interact with the interface. Most of the wave packet is reflected as can be seen when the wave packet passes through the atomic plane 90 between t=0.6 and 1.0 again. Part of the wave packet scatters inelastically and passes across the interface at a much lower frequency as can be seen from the slow oscillation of atoms in plane 122 between t=0.4 and 0.7.

During the initial interaction of the wave packet with the interface, the atomic planes on either side of the interface, planes 119 and 120, are not quite 180 degrees out of phase. Shortly after the wave packet is reflected/transmitted at t=0.7, the atomic planes 119 and 120 are exactly 180 degrees out of phase indicating a localized vibrational mode. The energy of this vibrational mode continues to decrease over time and releases energy to both side of the interface, which can be seen in Fig. 10(b). The localized vibrational mode inelastically scatters into lower frequency vibrational modes on the heavy side of the interface as can been seen in Fig. 10(b). This analysis clearly indicates two transport mechanisms, acoustic-acoustic and acoustic-localized-acoustic inelastic phonon scattering. These mechanisms are not accounted for by the models based on harmonic interatomic interactions. These additional scattering mechanisms can account for the improved overall energy transmission for the alloyed and lattice mismatch cases simulated above.

Although a single wavelength phonon wave packet was used in this simple computer experiment, the transmission across the interface was over 1.5% for a very low lattice perturbation. Values of over 10% have been reached for large amplitude wave packets. One can easily imagine that when a range of frequencies is considered, there can be multiple inelastic scattering possibilities, so that potentially a high transmission coefficient could be obtained.

Conclusions

The molecular-dynamics method was used to investigate thermal boundary resistances. A simple interface was created between two FCC materials. Simulations were conducted to determine the h_{BD} relationships to material mismatch and temperature. There was a strong temperature dependence, which suggests contribution of inelastic scattering to the energy transport through the interface. Further tests were conducted for interfaces with different atomic structures. In general, the disorder/defects were found to assist the energy transport, further supporting inelastic scattering as a major contributor to
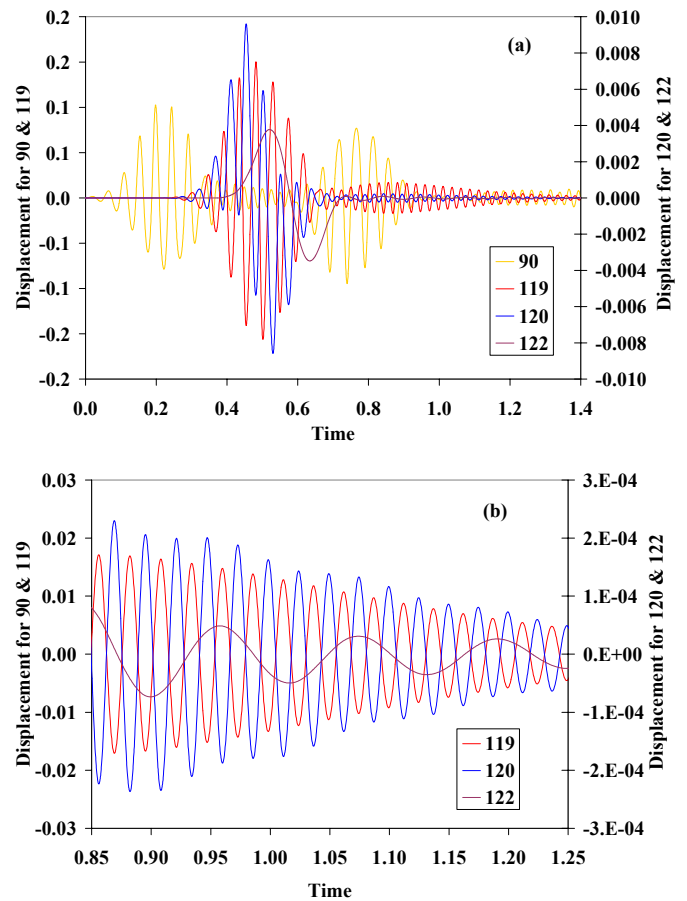

Fig. 10 Displacement of four atomic planes (90, 119, 120, 122) during the propagation of a longitudinal phonon wave packet. The interface is located between planes 119 and 120. Figure (b) shows the localized vibrational mode and its loss of energy over time.

the transport of thermal energy across an interface. Inelastic scattering was directly observed by releasing a wave packet near an interface and analyzing the displacements of atomic planes. Two inelastic scattering transport mechanisms were observed, one of which involves localized vibrations at the interface.

The simulations presented in this paper point to some of the shortfalls of simple harmonic models. Currently the simulations are being expanded to use other potentials (embedded atom model and Stillinger-Weber) and add electron bulk and interface scattering. A more extensive range of defects is being considered and may explain the overprediction of the DMM for Debye-like material interfaces. Phonon wave packet analysis will also continue to be used to try to better understand the regimes for which the above two inelastic scattering mechanisms are critical.

Acknowledgements

References

[1]   Kapitza, P.L., 1941, "The study of heat transfer in Helium II," Zhurnal eksperimentalnoi i teoreticheskoi fiziki, **11,** pp. 1-31.

[2]   Cahill, D.G., A. Bullen, and S.-M. Lee, 2000, "Interface thermal conductance and the thermal conductivity of multilayer thin films," High Temperature-High Pressures, **32,** pp. 135-142.

[3]   Mahan, G.D. and L.M. Woods, 1998, "Multilayer thermionic refrigeration," Physical Review Letters, **80,** pp. 4016-4019.

[4]   da Silva, L.W. and M. Kaviany, 2004, "Micro-thermoelectric cooler: interfacial effects on thermal and electrical transport," International Journal of Heat and Mass Transfer, **47,** pp. 2417-2435.

[5]   Phelan, P.E., 1998, "Application of diffuse mismatch theory to the prediction of thermal boundary resistance in thin-film high-Tc superconductors," Journal of Heat Transfer, **120,** pp. 37-43.

[6]   Phelan, P.E. et al., 1994, "Film/substrate thermal boundary resistance for an Er-Ba-Cu-O High-Tc thin film," Journal of Heat Transfer, **116,** pp. 1038-1041.

[7]   Cahill, D.G., 1997, "Heat transport in dielectric thin films and at solid-solid interfaces," Microscale Thermophysical Engineering, **1,** pp. 85-109.

[8]   Kim, E.-K. et al., 2000, "Thermal boundary resistance at Ge2Sb2Te5/ZnS:SiO2 interface," Applied Physics Letters, **76,** pp. 3864-3866.

[9]   Khalatnikov, I.M. and I.N. Adamenko, 1973, "Theory of the Kapitza temperature discontinuity at a solid body-liquid helium boundary," Soviet Physics JETP, **36,** pp. 391-387.

[10]   Swartz, E.T. and R.O. Pohl, 1989, "Thermal boundary resistance," Reviews of Modern Physics, **61,** pp. 605-668.

[11]   Cahill, D.G. et al., 2003, "Nanoscale thermal transport," Journal of Applied Physics, **93,** pp. 793-818.

[12]   Little, W.A., 1959, "The transport of heat between dissimilar solids at low temperatures," Canadian Journal of Physics, **37,** pp. 334-349.

[13]   Swartz, E.T. and R.O. Pohl, 1987, "Thermal resistance at interfaces," Applied Physics Letters, **51,** pp. 2200-2202.

[14]   Eisenberger, W., "Phonon scattering at surfaces and interfaces," in *Phonon Scattering in Condensed Matter V*, A.C. Anderson and J.P. Wolfe, Editors. 1986, Springer: Berlin/Heidelberg/New York. pp. 204.

[15]   Prasher, R.S. and P.E. Phelan, 2001, "A scattering-mediated acoustic mismatch model for the prediction of thermal boundary resistance," Journal of Heat Transfer, **123,** pp. 105-112.

[16]   Burkhard, G., A.B. Sawaoka, and P.E. Phelan, 1995, "The effect of Umklapp-processes on the heat transport of solids," *Proc., The Symposium on Thermal Science and Engineering in Honor of Chancellor Chang-Lin Tien*, eds., University of California Berkeley, California, pp. 145-152.

[17]   Stoner, R.J. and H.J. Maris, 1993, "Kapitza conductance and heat flow between solids at temperatures from 50 to 300 K," Physical Review B, **48,** pp. 16 373-16 387.

[18]   Stevens, R.J. et al., 2003, "Thermal boundary resistance of thin metal films and thermally conductive dielectric materials," *Proc., 2003 ASME International Mechanical Engineering Congress & Exposition*, ASME, eds., ASME, Washington, DC, pp. 41856_1-7.

[19]   Sergeev, A., 1999, "Inelastic electron-boundary scattering in thin films," Physica B, **263,** pp. 217-219.

[20]   Sergeev, A.V., 1998, "Electronic Kapitza conductance due to inelastic electron-boundary scattering," Physical Review B, **58,** pp. R10199-10202.

[21]   Huberman, M.L. and A.W. Overhauser, 1994, "Electronic Kapitza conductance at a diamond-Pb interface," Physical Review B, **50,** pp. 2865-2873.

[22]   Majumdar, A. and P. Reddy, 2004, "Role of electron-phonon coupling in thermal conductance of metal-nonmetal interfaces," Applied Physics Letters, **84,** pp. 4768-4770.

[23]   Young, D.A. and H.J. Maris, 1989, "Lattice-dynamical calculation of the Kapitza resistance between fcc lattices," Physical Review B, **40,** pp. 3685-3693.

[24]   Pettersson, S. and G.D. Mahan, 1990, "Theory of the thermal boundary resistance between dissimilar lattices," Physical Review B, **42,** pp. 7386-7390.

[25]   Kechrakos, D., 1991, "The role of interface disorder in thermal boundary conductivity between two crystals," Journal of Physics: Condensed Matter, **3,** pp. 1443-1452.

[26]   Fagas, G. et al., 1999, "Lattice-dynamical calculation of phonon scattering at a disordered interface," Physica B, **263-264,** pp. 739-741.

[27]   Pickett, W.E., J.L. Feldman, and J. Deppe, 1996, "Thermal transport across boundaries in diamond structure materials," Modelling Simulation in Materials Science and Engineering, **4,** pp. 409-419.

[28]   Maiti, A., G.D. Mahan, and S.T. Pantelides, 1997, "Dynamical simulations of nonequilibrium processes - heat flow and the Kapitza resistance across grain boundaries," Solid State Communications, **102,** pp. 517-521.

[29]   Daly, B.C. et al., 2002, "Molecular dynamics calculation of the thermal conductivity of superlattices," Physical Review B, **66,** pp. 024301 1-7.

[30]   Schelling, P.K., S.R. Phillpot, and P. Keblinski, 2002, "Phonon wave-packet dynamics at semiconductor interfaces by molecular-dynamics simulation," Applied Physics Letters, **80,** pp. 2484-2486.

[31]   Twu, C.-J. and J.-R. Ho, 2003, "Molecular-dynamics study of energy flow and the Kapitza conductance across an interface with imperfection formed by two dielectric thin films," Physical Review B, **67,** pp. 205422 1-8.

[32]   Berendsen, 1984, "Molecular dynamics with coupling to an external bath," Journal of Chemical Physics, **81,** pp. 3684-3690.

[33]   Schelling, P.K., S. Phillpot, and P. Keblinski, 2002, "Comparison of atomic-level simulation methods for computing thermal conductivity," Physical Review B, **65,** pp. 144306 1-12.